Journal of Physics D: Applied Physics

Prebreakdown and breakdown characteristics of stainless steel electrodes in vacuum

To cite this article: D W Williams and W T Williams 1974 *J. Phys. D: Appl. Phys.* **7** 1173

View the article online for updates and enhancements.

You may also like

- Prebreakdown Phenomena and Formation Processes of Low-Pressure Glow Discharges in Ar, Ar/N_2 and Ar/O_2 Mixtures
Tatsuzo Hosokawa, Kazuhiro Goto, Mikio Ohuchi et al.

- Structural evolution and thermal runaway of refractory W and Mo nanotips in the vacuum under high electric field from PIC-ED-MD simulations
Xinyu Gao, Nan Li, Andreas Kyritsakis et al.

- Photographic Observation System for DC Prebreakdown Phenomena in Dielectrics Using the Long Image Guide Scope
Kazunori Kadowaki Kazunori Kadowaki, Shinichi Arikawa Shinichi Arikawa, Sakae Nishimoto Sakae Nishimoto et al.

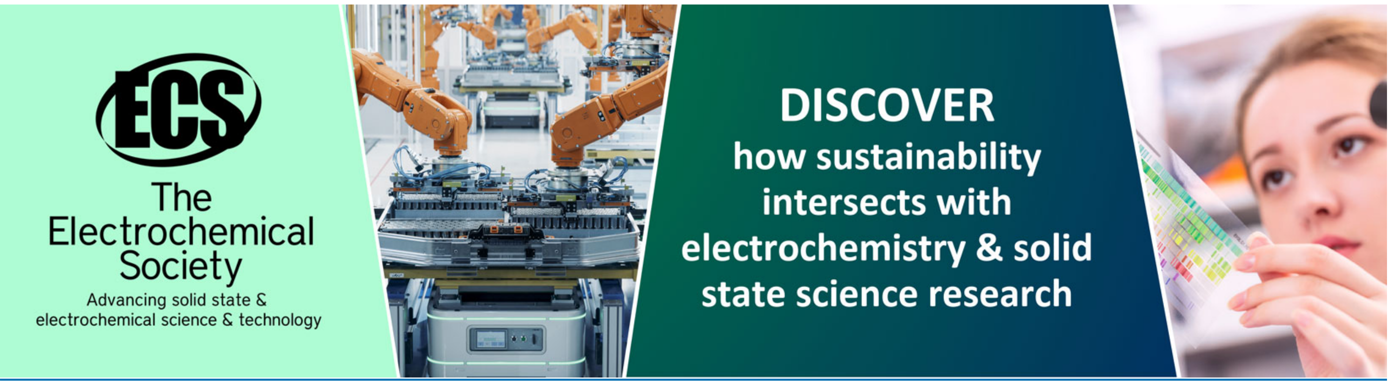

This content was downloaded from IP address 18.118.126.241 on 27/04/2024 at 21:03

J. Phys. D: Appl. Phys., Vol. 7, 1974. Printed in Great Britain. © 1974

Prebreakdown and breakdown characteristics of stainless steel electrodes in vacuum

D W Williams† and W T Williams
Department of Physics, University College of Swansea, Singleton Park, Swansea, SA2 8PP

Received 13 December 1973, in final form 31 January 1974

Abstract. Measurements of prebreakdown current as a function of applied electric field have been made for polished stainless steel electrodes in vacuum ($\sim 10^{-8}$ mm Hg) for gap separations $0{\cdot}02 < d < 0{\cdot}1$ cm. Experimental data were obtained (*a*) before the electrodes were outgassed, (*b*) after outgassing at 300 °C, (*c*) after conditioning the electrodes be repeated sparking, (*d*) after reversing the polarity of the electrodes, and (*e*) after restoring the polarity to its original mode. The data were analysed on the basis of the Fowler–Nordheim field emission theory. The breakdown voltage, the current at initiation of the discharge, the field enhancement factor, and the current density and emitting area at breakdown are given as a function of the number of breakdowns. The geometry and dimensions of the cathode microprotrusions are deduced. Results indicate that outgassing is necessary to achieve a stable surface, and that repeated sparking only conditions one electrode. Reversing the polarity destroys all conditioning effects. The variation of V_s with d would seem to indicate that the discharge was initiated by electron beams from the cathode producing electrode vapour at the anode.

1. Introduction

The prime aim of vacuum insulation is to avoid the occurrence of electrical breakdown between the components being insulated by the vacuum while at the same time maintaining the highest possible voltage between them. Recent publications by the authors (Williams and Williams 1972b, 1973) have shown that the breakdown voltage between two outgassed electrodes in a vacuum can be improved by repeated sparking of the discharge gap. This is recognized as a general method of 'conditioning' the electrodes to give reproducible results.

Many authors (eg Owen *et al* 1968, Powell and Chatterton 1970) have shown that the functional dependence of prebreakdown currents flowing in a discharge gap in vacuum on physical parameters such as the applied electric field and the surface work-function, etc is in accordance with the Fowler–Nordheim field emission theory (Fowler and Nordheim 1928). The electron emission occurs at microprojections on the cathode surface at which the applied electric field is enhanced locally. For a given applied voltage the field-emitted current remains constant; then, as the voltage is increased, the current also increases exponentially, but remains constant for a given voltage. However, if the voltage is increased sufficiently, then at a critical voltage called the breakdown voltage

† Now at Admiralty Surface Weapons Establishment, Portsmouth, Hants.

the steady prebreakdown current increases temporally and a spark occurs, resulting in electrical breakdown of the discharge gap. Several aspects of this transition are discussed by Hawley and Zaky (1967).

The experimental data obtained in the present work are analysed on the basis of the Fowler–Nordheim field emission equation. In addition to recording the values of the breakdown voltage V_s, and the current at which breakdown is initiated I_s, the following parameters were deduced: β, the factor by which the microscopic field at the cathode exceeds the average electric field E in the gap; A_s, the effective emitting area at breakdown; J_s, the corresponding current density; and F_s, the electric field at the tip of the microprojection when breakdown occurs.

In this work the first effect examined was the influence on the breakdown characteristics of outgassing the electrodes at a fairly low temperature (300 °C). The electrodes were then conditioned by sparking, and the effect of reversing the polarity of the electric field was investigated. On the basis of the experimental data obtained, an attempt was made to deduce information concerning the nature of the cathode microprojections. Finally, the variation of V_s with d was examined.

2. Apparatus

2.1. Discharge chamber and vacuum system

Figure 1 is a diagram of the discharge chamber. The chamber consists of a Pyrex glass tube, joined at one end to a stainless steel linear motion drive.

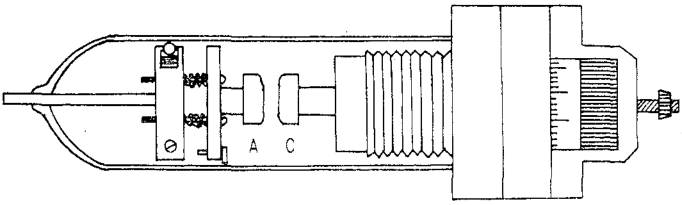

Figure 1. Discharge tube: total length, 18 cm; diameter of Pyrex glass tube, 3·5 cm. Electrodes: A, anode; C, cathode; diameter of each electrode, 1·5 cm.

The stainless steel electrodes were machined from a rod of type 303 stainless steel to a Rogowski profile, thus providing a uniform field configuration for gap separations up to 0·3 cm. The surface of each electrode was polished successively with polishing Alumina, grades 5/20 and 3/20, and finally with gamma-grade Alumina. This produced a mirror-like finish. Before being inserted in the chamber, they were, as were all components, cleaned with grease-removing solvents, then with distilled water, and finally dried.

Each electrode was screwed on to separate stainless steel supports. The cathode support was part of the linear motion drive, and the anode support was fixed to a frame held rigidly inside the chamber by means of spring-loaded ball bearings. Electrical connection to the anode was made by means of a tungsten rod projecting through the Pyrex glass. The anode was set parallel to the cathode by means of three levelling screws, and, with the aid of a travelling microscope, the gap could be set to a predetermined separation to within $\pm 3\%$. In this experiment the gap separation ranged from 0·02 to 0·1 cm.

The discharge tube was connected to a stainless steel ultra-high-vacuum system and evacuated by an absorption pump and two getter-ion pumps. It was possible to outgas the entire system at 300 °C by placing it in an oven. The base pressure in the system before outgassing was $\sim 10^{-8}$ Torr.

2.2. Electrical measuring circuit

The electric field was supplied by a 0–50 kV Brandenburg DC generator with a stability of 1 in 10^4. This was connected to the anode of the discharge gap via a 10^6 Ω resistor. The value of the voltage applied to the electrodes was deduced by means of a potential divider circuit, the potential drop across part of the resistor chain being continuously monitored against the EMF of a standard cell. Interelectrode currents in the range 10^{-12}–10^{-7} A were measured by means of a valve electrometer, and in the range 10^{-7}–10^{-3}A by a Scalamp galvanometer.

3. Experimental procedure

The voltage applied to the discharge gap was increased slowly from zero until a current of 10^{-12}–10^{-11} A flowed between the electrodes. Thereafter the voltage was increased in small steps of a few hundred volts, the values of V (and hence the electric field E) and I being recorded at each step. Initially the voltage was switched off before attaining the value of the breakdown voltage, but when conditioning the electrodes the voltage was increased until the discharge gap broke down and a spark was seen to pass between the electrodes. The entire experiment was carried out according to the following programme.

(*a*) Before the electrodes were outgassed, several E–I characteristics were obtained at different gap separations. In each case the voltage was increased until the current in the gap reached 10^{-4} A, at which value V was less than V_s. The voltage was then switched off and the next characteristic obtained by again starting at a low value of V.

(*b*) The electrodes were outgassed at 300 °C for 24 h, and after allowing them to regain room temperature in vacuum, the procedure described above was repeated several times, again switching off the applied field when $I = 10^{-4}$ A.

(*c*) The voltage was then increased until breakdown occurred, and with the gap separation kept constant at 0·06 cm, forty E–I characteristics were obtained, each one terminating in a spark breakdown.

(*d*) The polarity of the electrodes was reversed, and with $d = 0{\cdot}06$ cm, ten characteristics were obtained, again each one terminating in a spark.

(*e*) Finally, the original polarity was restored, and with d still fixed at 0·06 cm, forty characteristics were obtained, each one terminating in a spark.

4. Analysis

4.1. The breakdown parameters

The experimental data obtained by the above procedures were analysed according to the Fowler–Nordheim field emission equation

$$J = \frac{1{\cdot}54 \times 10^{-6} \beta^2 E^2}{\phi\, t^2(y)} \exp\left(-\frac{6{\cdot}83 \times 10^7 \phi^{3/2} v(y)}{\beta E}\right) \tag{1}$$

where J is the current density, E is the applied electric field, β is the field magnification factor at microprojections on the cathode surface, ϕ is the workfunction of the cathode material, and $t(y)$ and $v(y)$ are functions of the variable

$$y=\frac{3{\cdot}79\times10^{-4}\,(\beta E)^{1/2}}{\phi}$$

whose values have been tabulated (Good and Muller 1956). If the current I is emitted uniformly over an area A, then equation (1) can be rearranged as

$$\frac{I}{E^2}=\frac{1{\cdot}54\times10^{-6}\,\beta^2 A}{\phi\,t^2(y)}\exp\left(-\frac{6{\cdot}83\times10^7\phi^{3/2}v(y)}{\beta E}\right) \tag{2}$$

so that a semilogarithmic graph of $\ln(I/E^2)$ against $1/E$ should give a straight line of gradient m, where

$$m=-\frac{6{\cdot}83\times10^7\phi^{3/2}s(y)}{\beta}$$

$s(y)$ being another function of the variable y.

With the assumption that the cathode workfunction remains constant at 4·4 eV (see §5.2), β was determined from the gradient of the experimental graph. Using this, $F_s(=\beta E_s)$, the enhanced field at breakdown, was deduced. Since I_s, the current at which breakdown is initiated, was measured, values of J_s and A_s, the current density and emitting area at breakdown, could be deduced using equations (1) and (2).

4.2. *Geometry of the cathode microprojection*

The above parameters may be used to deduce information about the surface microgeometry. Alpert *et al* (1964) have shown that for a large number of projections, the one which gives the greatest value of β is predominant. The calculation used here deduces the geometry and size of the predominant projection. If there is no dominant projection, the experimental values of A_s will be so large as to render the calculation ineffective.

In a previous paper (Williams and Williams 1972a) two geometries were considered: a cylinder surmounted by a hemispherical cap, and a truncated cone also surmounted by a hemispherical cap. Three possible energy exchange processes occurring at the protrusion were examined: thermal conduction, resistive heating, and field emission heating (Nottingham 1941). The analysis in the previous paper was for molybdenum electrodes. In the present work, the analytical procedure is the same except that the physical constants for steel had different values from those of molybdenum. The following values were used for steel: thermal conductivity, 0·16 W cm^{-1} K^{-1}; resistivity, $70{\cdot}5\times10^{-6}$ Ω cm; coefficient of increase of resistivity, $1{\cdot}04\times10^{-3}$ K^{-1}. The value of the enhanced breakdown field F_s was taken to be $5{\cdot}5\times10^7$ V cm^{-1} (see §5).

When these three energy exchange processes are simultaneously active, instability leading to electrical breakdown occurs in a stainless steel cathode protrusion when the breakdown current is described by the following equations:

For a cylindrical emitter

$$I_s=6{\cdot}22\times10^2\,\frac{r}{\beta-2} \tag{3}$$

For a conical emitter

$$I_s=1{\cdot}68\times10^3\,r\cot\theta\,(1-\cos\theta)\left(1-\frac{\cot\theta}{2(\beta-5)}\right)^{-1}. \tag{4}$$

Here r is the radius of the hemispherical cap in each case, and θ is the half-angle of the cone.

The value of r may be calculated from the emitting area (Dyke and Dolan 1956), and since I_s and β are known, the geometrical nature of the protrusions may be deduced using equations (3) and (4) and a range of values for θ. The height h of a protrusion was also deduced from the relationship between β, h and r (Chatterton 1966); that is, for a cylinder $\beta=2+h/r$, and for a cone $\beta=5+h/2r$.

4.3. *Variation of V_s with d*

Maitland (1961) considered the production of metal vapour at the anode by bombardment of the surface by the field-emitted electron beam and obtained the breakdown criterion

$$V_s=kd^{\alpha}$$

where k and α are constants, and $\alpha=0{\cdot}8$. A test of the electron-beam-initiated breakdown theory is thus a measurement of the linearity of the graphs of $\ln V_s$ against $\ln d$ and an assessment of α.

For this reason, V_s was measured as a function of d both for unconditioned and conditioned electrodes in the present work.

5. Results

It is convenient to discuss the results in relation to the experimental programme outlined in §3.

5.1. *Pre-outgassing*

The current I was measured as a function of the applied field E for gap separations $0{\cdot}02<d<0{\cdot}1$ cm. Some of the E–I characteristics are shown in figure 2(*a*), and the corresponding Fowler–Nordheim graphs in figure 2(*b*). All the graphs were characterized by discontinuities. Experimentally, these discontinuities were recognized as a rapid stepwise change in the current at a steady applied field. The current could change by as much as an order of magnitude, but would remain at this new value until the field was altered.

Between the discontinuities, the Fowler–Nordheim graphs were straight lines of different gradients, and at almost every transition, β would increase and A decrease; eg the values of β and A given in table 1 refer to the graph obtained at $d=0{\cdot}05$ cm shown in figure 2(*b*).

5.2. *After outgassing, but preconditioned*

After outgassing the electrodes at 300 °C and allowing the temperature of the electrodes to return to room temperature, E–I characteristics were again obtained for the same range of d as in §5.1. For ease of comparison, these are also shown in figure 2(*a*) and the corresponding Fowler–Nordheim graphs in figure 2(*b*). For a given gap separation and a given applied field, the current was reproducible to within 30% even after the apparatus had been switched off overnight.

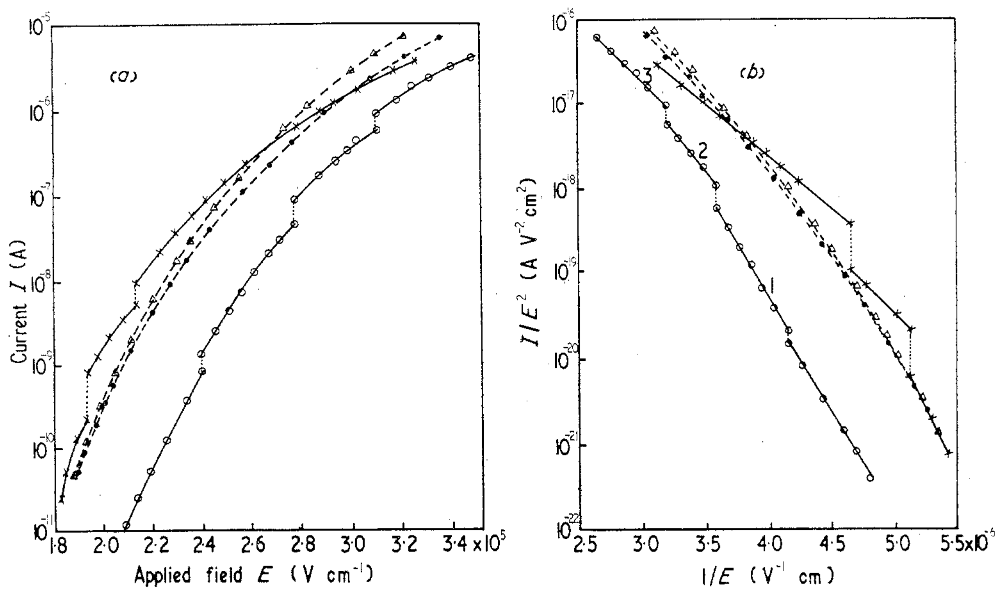

Figure 2. (*a*) Typical *E–I* characteristics and (*b*) typical Fowler–Nordheim graphs for unoutgassed electrodes (————) and for outgassed but unconditioned electrodes (– – – –): ○, d=0·05 cm; ×, d=0·07 cm; △, d=0·02 cm; ●, d=0·06 cm.

Table 1. Values of β and A calculated from the Fowler–Nordheim graph at d=0·05 cm

Section of graph	β	A (cm^2)
1	101	$7{\cdot}8\times10^{-7}$
2	152	$3{\cdot}3\times10^{-10}$
3	209	$7{\cdot}8\times10^{-12}$

Very few current discontinuities were observed after outgassing, and most of the Fowler–Nordheim graphs were smooth curves, as can be seen from figure 2(*b*). Curved Fowler–Nordheim graphs have been reported by Rohrbach (1966) for large d ($1<d<10$ cm), but the curvature was in the opposite direction. However, Watts (1961) has observed curvature in the same direction as in the present work.

It is pertinent to note that the gap separation was remeasured on several occasions when the current was slightly less than I_s, ie at an applied field of $\sim 4\times10^5$ V cm^{-1}, and on each occasion it was found that the separation had decreased due to the electrostatic force acting on the electrodes, thus extending the bellows in the linear motion drive. This decrease in d only occurred towards the upper limit of the applied field and introduced an error of 18% into the values of E at these large values. But even when the reduction in separation was taken into account, the Fowler–Nordheim graph was still curved.

The curvature could be due to both β and ϕ varying with increasing current. If it was assumed that β remained constant, then calculation showed that ϕ decreased with increasing current by 35% of its original value of 4·4 eV. Since it does not seem physically possible that the workfunction of the metal surface could change by this amount during the course of the experiment, it was assumed that ϕ remained constant and that, in the case of a curved Fowler–Nordheim graph, β varied. This, of course, is physically possible, since a projection can become sharper or blunter during an experiment. Typical plots of β against E are shown in figure 3(*a*) together with the value of the emission area A, which also altered with the applied field.

The variation of β with d for a given applied field was calculated, and the values showed that, for a given field, β decreased with increasing d. The variation of β with d is shown in figure 3(*b*).

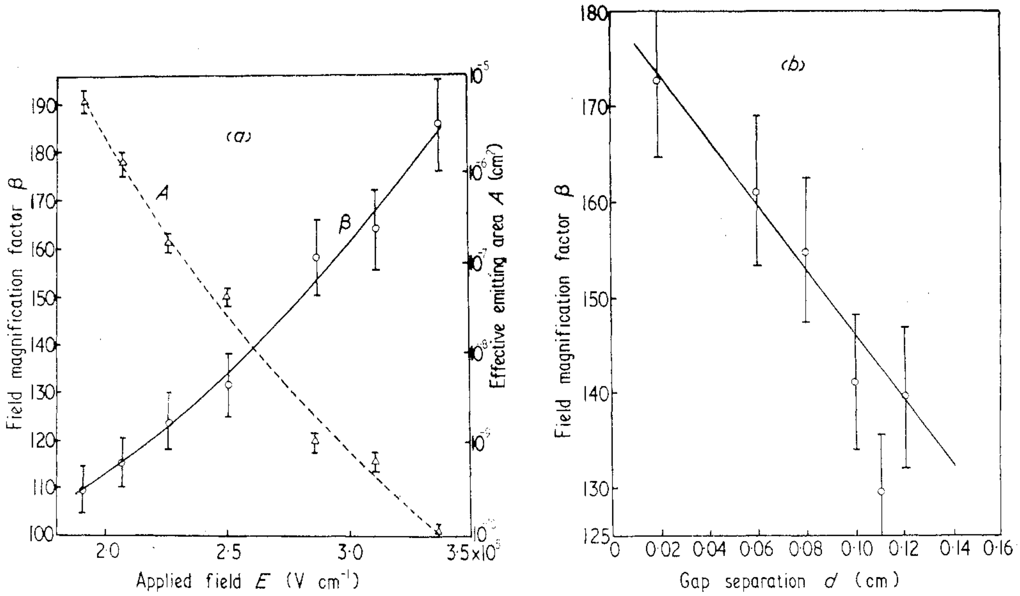

Figure 3. (*a*) Variation of field magnification factor β (———) and effective emitting area A (- - -) with applied field for constant gap separation d=0·06 cm. (*b*) Variation of field magnification factor β with gap separation d for a constant applied field $E=3\times10^5$ V cm^{-1}.

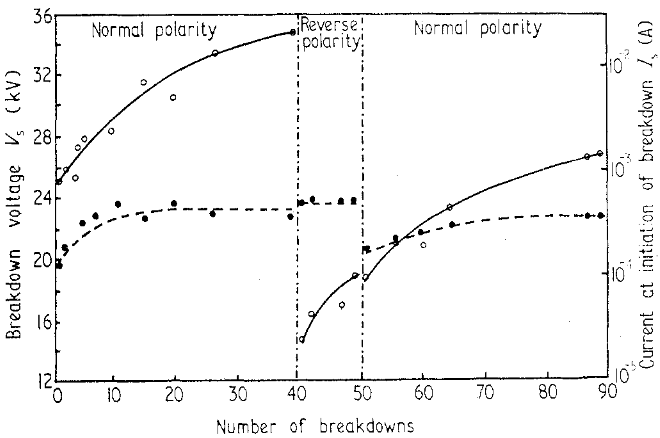

Figure 4. Variation of breakdown voltage V_s (○, —) and current at initiation of breakdown I_s (●, - - -) with number of breakdowns for normal and reverse polarity; d=0·06 cm.

5.3. *Conditioned electrodes*

5.3.1. Normal polarity. During this part of the experiment, each *E–I* characteristic terminated in spark breakdown, and forty such characteristics were recorded, all at a fixed gap separation of 0·06 cm. After the third breakdown, the Fowler–Nordheim graphs were straight lines. The breakdown voltage increased from 25·3 to 35 kV during the experiment, while I_s also increased from 10^{-4} to a constant value of $3{\cdot}5 \times 10^{-4}$ A. The values of V_s and I_s are shown in figure 4. The values of β, F_s, A_s and J_s calculated from the graphs are shown in figures 5 and 6. For convenience the data discussed in §5.3.2 and §5.3.3 are also shown in figures 4–6.

The geometry and dimensions of the cathode microprotrusion which gave the best fit for the data of the experiment ending in the first breakdown were that of a conical protrusion of half-angle 4°, height 9 μm, and tip radius 3×10^{-6} cm. Repeated sparking

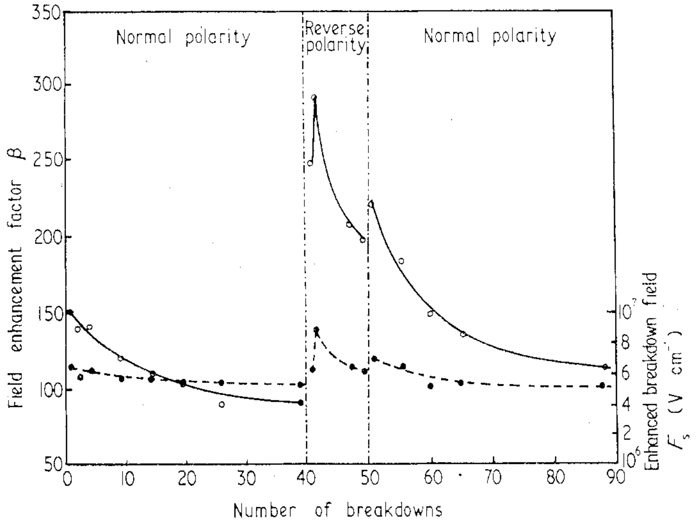

Figure 5. Variation of field magnification factor β (○, —) and enhanced breakdown field F_s (●, - - -) with number of breakdowns for normal and reverse polarity; $d = 0{\cdot}06$ cm.

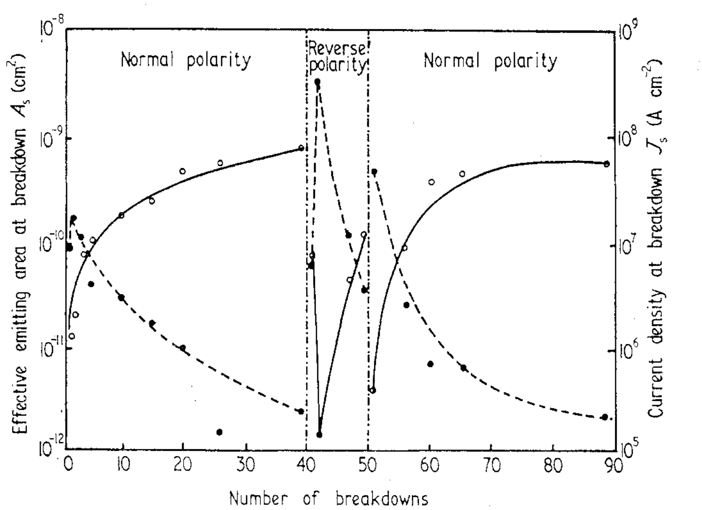

Figure 6. Variation of effective emitting area A_s (○, —) and current density J_s (●, - - -) at breakdown with number of breakdowns for normal and reverse polarity; $d = 0{\cdot}06$ cm.

produced longer, sharper cones, until after twenty breakdowns the cone had a half-angle of 1°, height 38 μm, and tip radius 2×10^{-5} cm. Eventually the microprotrusion became cylindrical, and for the last breakdown had a height of 29 μm and tip radius 3×10^{-5} cm.

5.3.2. Reverse polarity. The polarity of the electrodes was reversed, and ten *E–I* characteristics were obtained. All the Fowler–Nordheim graphs were straight lines. The initial value of the breakdown voltage had decreased to 15 kV, but this increased to 18·8 kV with sparking. The variation of all the parameters is shown in figures 4–6.

The cathode microgeometry remained conical throughout, with the height remaining constant at 37 μm and the tip radius at 8×10^{-6} cm. The half-angle decreased slightly from 4° to 2°.

5.3.3. Normal polarity. The polarity was reversed to the original mode, and a further forty *E–I* characteristics obtained. It became immediately apparent that reversing the polarity the first time had 'unconditioned' the surfaces, since the current was unstable and many discontinuities occurred in the characteristics. After a few breakdowns it became more stable. The initial value of V_s was 18 kV, and after forty breakdowns it was only 26 kV. The variation of the parameters is shown in figures 4–6.

The initial microgeometry was deduced to be a low, flat cone with half-angle 7°, height 7 μm, and tip radius 2×10^{-6} cm. Eventually this became a cone of half-angle $\frac{1}{2}$°, height 48 μm, and tip radius 2×10^{-5} cm, and by the 38th breakdown had become a cylinder of height 20 μm and tip radius 2×10^{-5} cm.

5.4. Variation of V_s with d

Two graphs of ln V_s against ln *d* were drawn, the first after the electrodes were outgassed but before sparking, and the second after conditioning the gap by repeated sparking. These are shown in figure 7. In both cases straight lines were obtained, the gradient in the first case being 0·9 and in the second 1·0.

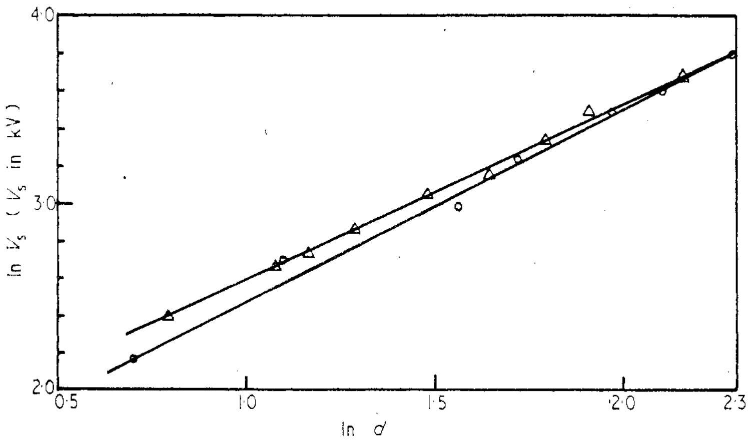

Figure 7. Variation of ln V_s with ln *d* for outgassed but unconditioned electrodes (△) and for conditioned electrodes (○): △ slope=0·92; ○ slope=1·01.

6. Conclusions and discussion

(i) Before outgassing the electrodes, there were discontinuities in the E–I characteristics due to the current changing at a steady value of the electric field. This would suggest the addition or elimination of emissive sites (Little and Whitney 1963). The increasing β and decreasing A usually associated with the discontinuities would suggest that the projections became larger and sharper, or that new sharp projections suddenly appeared on the cathode surface.

(ii) Outgassing the electrodes produced a more stable surface, and the prebreakdown current was consistent with the Fowler–Nordheim relationship provided that β increased with increasing applied field. This would suggest that the existing protrusion became sharper as the field increased, due to migration of material from the base. An increase in E produces a net outward force on the protrusion, and at the same time the surface tension and tensile strength of the material decrease due to the increase in temperature as I increases.

(iii) Sparking the electrodes served to destroy those protrusions with a high β, thus increasing V_s and conditioning the electrodes. The change of microgeometry with sparking confirmed this view. Continued sparking increased the height and decreased the half-angle of the initial conical protrusions. Since the increase in r is greater than the increase in h, then β decreases. Eventually, the microprojection becomes cylindrical and β, h and r remain sensibly constant, thus providing a conditioned gap. These results are in agreement with earlier work on molybdenum electrodes (Williams and Williams 1972b, 1973).

(iv) Reversing the polarity changed the values of β and V_s, and it would appear that 'conditioning the gap' really implies conditioning one electrode only. The full process of conditioning by sparking must be carried out in the reverse polarity mode to obtain constant results. However, when the polarity was restored to the original mode, observations indicated that all the conditioning effects produced originally had been destroyed. These results are consistent with those of Owen *et al* (1968).

(v) The slope of the two graphs of ln V_s against ln d were 0·9 and 1·0, and were in better agreement with the work of Maitland (1961) who predicted a slope of 0·8, than with the work of Slivkov (1957) and Cranberg (1952) who predicted a slope of 0·63 and 0·5 respectively. This would seem to indicate that for a gap separation in this range of d the discharge was initiated by electron beams from the cathode producing metal vapour at the anode. This again is in agreement with results obtained with molybdenum electrodes (Williams and Williams 1973).

Acknowledgments

The authors wish to express their gratitude to Professor C Grey Morgan for his guidance and helpful discussions, and to UKAEA, Aldermaston, for the award of a contract which enabled the work to be undertaken.

References

Alpert D, Lee D, Lyman E M and Tomaschke H E 1964 *J. Vac. Sci. Technol.* **1** 35
Chatterton P A 1966 *Proc. Phys. Soc.* **88** 231–45
Cranberg L 1952 *J. appl. Phys.* **23** 518–22

Davies D K 1973 *J. Vac. Sci. Technol.* **10** 115–21
Dyke W P and Dolan W W 1956 *Adv. Electron. Electron Phys.* **8** 90–5
Fowler R H and Nordheim L 1928 *Proc. R. Soc.* A **119** 173–81
Good R H and Muller E W 1956 *Handb. Phys.* **21** 181–91 (Berlin: Springer-Verlag)
Hawley R and Zaky A A 1967 *Prog. Dielect.* 7 115–215 (London: Heywood)
Little R P and Whitney W T 1963 *J. appl. Phys.* **34** 2430–2
Maitland A 1961 *J. appl. Phys.* **32** 2399–407
Nottingham W B 1941 *Phys. Rev.* **59** 907
Owen W D, Davies M H and Powell W D 1968 *Proc. 3rd Int. Symp. on Discharges and Electrical Insulation in Vacuum, Paris* (Paris: Dunod) pp 163–70
Powell H P S and Chatterton P A 1970 *Vacuum* **20** 419–29
Rohrbach F 1966 *Proc. 2nd Int. Symp. on Insulation of High Voltages in Vacuum* (Boston: MIT) pp 83–97
Slivkov I N 1957 *Sov. Phys–Tech. Phys.* **2** 1928–37
Watts C 1961 *PhD Thesis* University of Wales
Williams D W and Williams W T 1972a *J. Phys.* D: *Appl. Phys.* **5** 280–90
—— 1972b *J. Phys.* D: *Appl. Phys.* **5** 1845–54
—— 1973 *J. Phys.* D: *Appl. Phys.* **6** 734–43